1. Introduction

The earliest clinical manifestation of dental enamel caries is a white spot lesion (WSL), consisting of a porous lesion body and a relatively intact surface layer formed through re-precipitation of dissolved calcium and phosphate ions that are retained partially in the overlying dental plaque biofilm [1, 2]. It is believed that the WSL is reversible at its early stage if remineralisation processes can be instigated [3].

Remineralisation of carious lesions is "the delivery of calcium and phosphate from outside the tooth into the enamel lesion, effecting deposition of mineral onto demineralised enamel within" [4]. Numerous studies have established the anti-caries benefits of topical remineralising agents, including fluoride [5,6], nano-hydroxyapatites [7,8] and bioglass [9,10]. Milly et al. [11] studied enamel WSL remineralisation using bioglass modified with polyacrylic acid (PAA) which mimics the functional role of non-collagenous proteins in binding the calcium and phosphate ions to form nano-precursors. Significant mineral deposition occurred on the surface, with an insignificant reduction of the lesion depth. Other agents including fluoride and casein phosphopeptide-amorphous calcium phosphate (CPP-ACP) have also been investigated [12,13]. The preferential deposition of ions on the lesion surface occlude the surface porosities. This hinders ion complexes from infiltrating the porous subsurface, so restricting a more complete lesion consolidation [4,14]. Cochrane et al. [15] proposed a definition of remineralisation that "includes any crystal repair to bring about net mineral gain to an enamel subsurface lesion, but does not extend to precipitation of solid phases onto enamel surfaces". Therefore, the delivery of remineralising ions into deep lesion plays a crucial role in achieving optimal remineralisation [16].

In recent years, chitosan, an *N*-deacetylated derivative product of chitin, has attracted much attention with regards to it role in promoting enamel remineralisation. Chitosan has been used in dental biomaterials due to is ready availability, biocompatibility, biodegradability and non-toxicity [17,18,19,20,21]. Its positive charge permits adherence to the negatively charged demineralised enamel surface [22,23]. A study has revealed its ability to penetrate enamel [24], thus has the potential to carry mineral ions deeper into the lesion. In previous work, it has been shown that chitosan solution used as a pre-treatment on a porous lesion surface could promote subsurface remineralisation by Bioglass infiltration [25]. Chitosan hydrogel including amelogenin rP-172 could bring about biomimetic remineralisation on either erosive or carious enamel lesions [26,27].

In a further study, Ruan et al. found that chitosan-amelogenin (CS-AMEL) hydrogel could repair the incipient artificial enamel carious lesions by inducing the formation of oriented apatite crystals and reduction of the lesion depth [28]. Hence, chitosan has a potential to promote subsurface enamel remineralisation in conjunction with other biomaterials.

This study reports the development of a chitosan-bioglass complex material. The aim of this study was to investigate the efficacy of chitosan-bioglass complex to improve subsurface WSL lesion mineral deposition under both static and dynamic demineralisation-remineralisation regimes. To create a more clinically relevant model, a salivary pellicle was introduced. Raman intensity mapping, microhardness, scanning electron microscopy and energy dispersive X-ray spectroscopy were utilised to assess mineral gain, mechanical properties, ultrastructure and elemental composition, respectively, after remineralisation. The null hypothesis was that chitosan-bioglass complex cannot remineralise subsurface WSLs in either remineralisation model.

2. Materials & Methods

2.1 Incipient lesion formation

Sixty-four enamel slabs were sectioned from caries-free human molar teeth with ethics approval from the UK NHS Health Research Authority (Reference 16/SW/0220). Enamel slabs were included in acrylic resin (Oracyl^{TM}, Bracon, UK) and the exposed surface was polished (LabForce-100, Struers, Denmark) using P500 grit for 10 s, P1200 for 15 s, P2000 for 30 s and P4000 for 2 min. Ultrasonication was conducted for 1 min between each step and 4 min after P4000. A working window 1 mm wide and 3 mm long was created on the finished surface using nail varnish to block out the surrounding surfaces.

Artificial white spot lesions were formed using an acidic gel model consisting 8 wt% methylcellulose gel and 0.1 M lactic acid (pH 4.60, adjusted by 1M NaOH) [11]. Enamel samples were placed on the base of 250 mL glass beaker filled with 100 mL gel and an equal amount of lactic acid was added with a filter paper between the two layers. The demineralisation was performed in an incubator (MIR-262, Sanyo, Japan) at 37^{o}C for 21 days. Solutions were refreshed on a weekly basis. After formation, the acidic gel and nail varnish were carefully removed by deionised water and acetone, respectively, followed by rinsing under deionised water.

2.2 Group assignment

Lesion samples were separated equally for use in the two remineralisation models. In each model, samples were assigned to four groups (n = 8): (1) bioglass application on chitosan pre-treated lesions (CB); (2) chitosan-bioglass slurry (CBS); (3) "standard" remineralisation solution (RS – positive control); (4) deionised water (NC – negative control) (see table 1).

2.3 Baseline surface Raman intensity mapping

Baseline Raman surface intensity mapping was performed on five samples in each group. The acquisition was carried out using a micro-Raman spectrometer (inVia Raman Spectroscopy, Renishaw, UK) assembled with 1200 line/mm grating, using Streamline^{TM} mode at the laser wavelength of 785 nm. The scanning area included lesion and sound enamel on both sides and contained 91,000 acquisition points with a step size of 2.7 μm in x and y direction. The map was generated by monitoring the peak at 960 cm^{-1}, the strongest peak of phosphate group which is considered to be an indicator of mineral content [29].

After acquisition, all maps were analysed using in-house software. Intensity ratios of lesion/sound (I_{lesion}/I_{sound}) were calculated to indicate mineral content (which is assumed to be 100 % in sound enamel) through fitted peak height maps, using ImageJ (NIH, US).

2.4 Baseline surface microhardness

Surface Knoop microhardness was performed on the surface of the same samples used in Raman intensity mapping using a Knoop microhardness tester (Duramin, Struer, Denmark). With a load and dwell time of 10 gf and 5 s, respectively, 5 indentations measured with a spacing of at least 50 μm.

2.5 Collection of human saliva

Human whole saliva was collected from one medically fit and well subject. Eating and drinking were prohibited for at least 2 hours prior to collection. The subject was instructed to chew paraffin

gum to generate saliva. Saliva was then collected in a polystyrene tube (Sterilin™, Thermo Fisher Scientific, UK) and stored in -80ºC freezer. Before use, saliva was fully defrosted in a water bath at room temperature.

2.6 Static remineralisation

Sound enamel surrounding the artificial lesion was protected using acid-resistant tape. Pellicles were formed on the lesion surface by application of saliva for 3 min in a mini orbital shaker (SO5, Stuart Scientific, UK) at 62.5 RPM according to previously published protocols [30]. After completion, lesions were gently washed by deionised water to remove excessive saliva and then carefully dried using compressed air.

Static remineralisation was conducted by applying remineralising agents onto the lesion surface (CB and CBS groups) or immersing in solutions (RS and NC groups). Lesion samples were fitted into a 6-well plate. Formulations of all materials are shown in **Table 1**. For chitosan pre-treatment in CB group, 2.5 mg/mL chitosan solution prepared by dissolving chitosan powder in 0.1 M acetic acid was applied onto the lesion surface for 1 min, washed off and dried using compressed air. The remineralising agent was prepared by dissolving bioglass powder in deionised water to form a concentration of 1.0 g/mL. For the CBS group, chitosan-bioglass material was prepared by adding 2.5 mg/mL chitosan solution into bioglass powder to form a concentration of 0.5 g/mL and thoroughly mixing for 10 s using a whirlmixer. The concentration was decided from a previously conducted pilot study (see supplied information). All materials were applied immediately after formulation. To maintain humidity, a small amount of deionised water was added in the wells for CB and CBS. For RS and NC, samples were fully immersed in the solutions. The remineralisation was conducted for 7 days continuously. All materials including pellicle layer were refreshed on a daily basis.

2.7 pH-cycling regime

A clinically relevant pH-cycling regime was applied for 7 days to evaluate the remineralising efficacy of the chitosan-bioglass material as reported in previous work [30]. The cycling procedure is illustrated in **Figure 1**.

Sound enamel was protected with acid-resistant tape to avoid contaminants from treatment. Before each 3-min treatment phase, the formation of pellicle layer and the preparation of remineralising materials or solutions were carried out in the same fashion as described in **Section 2.6**. Samples in the CB group were pre-treated with 2.5 mg/mL chitosan solution for 1 min. The 3-min treatment was performed using a toothbrushing machine (Toothbrush, Syndicad, Germany) adapted with microbrush (Benda® Microtwin®, CENTRIX, Australia) at a speed of 1 stroke per second. Samples were fixed and remineralising agents or solutions were applied directly on lesion surface. After brushing, samples were rinsed thoroughly with deionised water. The acidic challenge was carried out using the same acidic gel system as described in the lesion formation.

After pH-cycling, samples were rinsed with running deionised water to remove any remnants on the lesion surface. Protection tape was removed, and samples were stored in deionised water at 4°C before characterisation.

2.8 Characterisations post-treatment

The same sample used for baseline testing were characterised by surface Raman intensity mapping post-treatment using the same method described in **Section 2.3**. The mineral content change was calculated as $\Delta I = [(I_{lesion}/I_{sound})_{post} - (I_{lesion}/I_{sound})_{before}] \times 100\%$.

Knoop microhardness (KHN) was performed on the same samples again using the same parameters as aforementioned. Subsequently, these samples were hemi-sectioned to reveal the lesion depth cross-sections. The cross-sections were further polished up to P4000 grade without ultrasonication cleansing. One half was assigned for cross-sectional depth microhardness assessment using the same KHN indentation protocol as above. Due to the limitation of lesion depth, only 3 indentations were measured for each sample with a 100 μm interval.

The remaining samples (n = 3) in each group were fractured into two parts. One half was used for lesion surface scanning electron microscopy (SEM) observation and the other used to examine the cross-sectional surface. These surfaces were sputter-coated with gold and imaged using a scanning electron microscope (JCM-6000, JEOL, Japan) in secondary electron mode with an acceleration voltage of 15 kV. Elemental analysis was carried out quantitatively using the built-in energy dispersive X-ray (EDX) spectrometer in back-scattered electron mode with the same

acceleration voltage. Three selected area acquisitions were performed on each sample, and Ca/P and Ca/Si atomic ratios were calculated.

2.9 Statistical analysis

All Raman and microhardness data were analysed statistically using one-way ANOVA with Tukey's test carried out in SPSS 23 for Windows (IBM, USA). Statistical significance was set at $P < 0.05$. Before ANOVA analysis, the normality and homogeneity of all data were checked by Shapiro-Wilk test and Levene test, respectively.

3. Results

3.1 Mineral regain

Mineral regain was indicated by the change of surface Raman intensity and summarised in **Table 2**. All experimental groups exhibited significant increase in surface mineral content compared to the negative control (0.00 ± 0.72) after 7d static remineralisation ($p < 0.05$). RS (9.07 ± 1.37) showed more increase than CB (5.11 ± 1.69) and CBS (5.01 ± 1.64). After pH-cycling, mineral content increased in all groups, among which CBS (14.46 ± 1.98) was the greatest, followed by CB (10.20 ± 1.30), NC (8.48 ± 2.22) and RS (7.57 ± 1.78).

3.2 Mechanical performance

Surface Knoop microhardness pre- and post-remineralisation are illustrated in **Figure 2**. Before remineralisation, artificial WSLs had an average surface microhardness of 66 KHN. As shown in **Figure 2a**, static remineralisation induced significant hardness recovery in all groups except NC ($p < 0.05$), in which the average hardness showed a decrease (-6.3 ± 10.0, KHN). The greatest hardness was found in CBS (185.0 ± 18.9). In comparison, all groups in the pH-cycling study exhibited a significantly better mechanical performance post-treatment ($p < 0.05$) (**Figure 2b**). Similarly, CBS had the greatest hardness (152.3 ± 10.1), followed by CB (142.4 ± 6.5), and both were superior to RS (90.9 ± 5.2) and NC (97.3 ± 5.1).

Due to the limitations of the study (discussed later), baseline cross-sectional microhardness for each group could not be ascertained. The assessment was carried out 20 μm subsurface and is

shown in **Figure 3**. Hardness reached 65.1 ± 8.9 and 56.7 ± 8.7 in CBS and CB groups, respectively, which was greater when compared to NC (12.7 ± 1.3) ($p < 0.05$), as revealed in **Figure 3a**. The "standard" remineralisation solution (positive control), in contrast, contributed little to rehardening the subsurface in RS (18.6 ± 5.8) ($p > 0.05$). The same trend was found after pH-cycling for 7 days (**Figure 3b**). Nevertheless, by comparing corresponding groups that went through two different remineralisation regimes, it was found that the average hardness was less in the pH-cycling than that in the static study for CB (40.1 ± 6.0) and CBS (52.7 ± 3.6), while slightly greater for RS (24.8 ± 3.4) and NC (24.3 ± 4.4).

3.3 Ultrastructural observations

The surface of CB samples exhibited dense morphology with small round crystals resulting from static remineralisation (**Figure 4a**). No enamel prism boundaries were observed. Interestingly, CBS showed a coarse surface consisting a number of spherical precipitations < 1 μm (**Figure 4b**) that covered the entire surface and were comprised of nanocrystals. No obvious porosities were observed. Remineralisation also induced precipitations on the surface in the RS group, as shown in **Figure 4c**. Compared subjectively to CB, the freshly deposited layer in RS was heterogeneous and more porous. In addition, crystals did not show clear orientation. In comparison, significant prism boundary along with porosities were clearly seen in NC as a consequence of demineralisation (**Figure 4d**). No precipitation or mineral deposition were evident from the surface morphologies in NC. It was also noticed that all groups except CBS showed the existence of scratches caused by the polishing process (black triangles).

After pH-cycling, CB exhibited a densely packed surface morphology (**Figure 6a**). The newly precipitated layer covering the entire surface was composed of round nano-sized crystals, showing no evidence of a classic prismatic appearance. Whereas in CBS, the surface was also covered by a newly deposited layer, which had a subjectively smoother appearance compared to CBS (**Figure 6b**). The morphology was denser, and the crystal size was smaller. No obvious sign of porosities was found in both groups. Although pH-cycling induced some precipitations in RS as revealed in **Figure 6c**, those newly grown minerals were patch-like and heterogeneous. The precipitated layer failed to cover the entire surface, leaving the boundary of enamel prisms exposed. NC group did

not exhibit a recognisable new precipitated layer (**Figure 6d**). The surface was still porous after treatment with scratches (black triangles).

Representative cross-section SEM micrographs after static remineralisation and pH-cycling are shown in **Figure 7** and **Figure 8**. Prisms in CB were covered by newly precipitated crystals extending at least 20 μm (**Figure 7a**). These crystals demonstrated an irregular distribution and were mostly configured as small spheres (**Figure 7b**). However, significant voids were still observed as indicated by the white arrow. CBS also exhibited extensive remineralisation across the subsurface investigated (red arrows, **Figure 6c**). Newly deposited crystals showed a tightly packed structure, increasing the density of the remineralised subsurface depth (**Figure 7d**). Additionally, the typical prismatic structure was absent in CBS, which could be found in RS (**Figure 6e**) and NC (**Figure 6g**). There was no significant evidence suggesting precipitation took place in the subsurface in NC. Orientation was somehow disrupted and a large number of pores were visible (**Figure 6h**). Similar features were observed in RS, with slightly denser structure (**Figure 6f**).

The subsurface of CB after pH-cycling treatment revealed significant precipitations all over the scanned area (**Figure 7a**). From the magnified observation, these precipitations were composed of flaky nanocrystals which were loosely deposited, leaving significant voids (**Figure 7b**). The precipitated layer was heterogeneous with some larger pores as indicated by white arrows (**Figure 7a**), which could be a result from the fracture process that destroyed the precipitation. It was surprising to see that the subsurface of CBS exhibited a significantly different morphology compared to that of CB (**Figure 6c**). Firstly, the entire subsurface was covered completely by the precipitation layer, showing no obvious porosities. Typical prismatic structure was absent. Secondly, plate-like crystals sized from nano- to micro-scale were found distributed randomly (red arrow). Close investigation revealed that the precipitation consisted of densely packed rod-like nanocrystals. In contrast, such a layer was not observed in RS and NC. Prismatic structures appeared in both groups with a lot of voids resulting from demineralisation (**Figure 7e** and **7g**). Crystals of the host tissue showed uniform orientation without obvious distortion (**Figure 7f** and **7h**).

3.4 Elemental composition

Ca/P and Ca/Si atomic ratios were calculated from EDX results and are summarised in **Table 3** and **Table 4**. In the static study, CBS showed a statistically significant higher Ca/P ratio after treatment, reaching 2.98 ± 0.38, compared to NC (1.70 ± 0.03) ($p < 0.05$), which was slightly higher than the stoichiometric value of pure HA (1.67). CB (1.89 ± 0.03) also had a statistically insignificant greater mean Ca/P than NC. No obvious difference was found between RS and NC. In regards of the subsurface Ca/P, the largest value was found in CB (1.81 ± 0.18). However, the standard deviation was high so there was no statistical difference when compared to NC (1.57 ± 0.02). CBS exhibited a higher average value of 1.67 ± 0.04 than both RS and NC.

After pH-cycling, however, it was noted that the highest surface Ca/P was in RS (1.84 ± 0.19), slightly greater than that in NC (1.75 ± 0.04), CB (1.69 ± 0.03) and CBS (1.68 ± 0.04) ($p > 0.05$). Whereas in the subsurface depth, the trend was reversed so that CB (1.68 ± 0.15) and CBS (1.68 ± 0.13) showed greater values than RS (1.57 ± 0.03) and NC (1.59 ± 0.10). It should be mentioned that the standard deviation was large (except RS) so that there was no statistical significance. Moreover, mean values of surface and subsurface were generally consistent in CB and CBS groups in both studies, and were close to that of pure HA. While for RS and NC, Ca/P was higher than 1.67 on surface due to remineralisation and weaker on subsurface because of demineralisation.

Table 4 gives the Ca/Si values of all groups. Only in CB and CBS groups after static remineralisation was silicon detected. Surface of CBS was found to have the relatively greatest amount of Si as the Ca/Si reached 5.04 ± 0.28. Subsurface of CBS also had a small Ca/Si ratio (9.86 ± 0.93). Nevertheless, it must be noted that Si was not detected in one out three samples used for this evaluation, and another sample had a Ca/Si >50 which was discarded as an outlier. Therefore, 9.86 ± 0.93 was the value from only one sample. CB showed less content of Si than CBS ($p < 0.05$). None of four groups was found to have silicon from bioglass after pH-cycling.

4. Discussion

The objective of enamel remineralisation is to deposit mineral back into the depth of the demineralised tissue to occlude the pores. The outermost surface zone of an enamel WSL has a mineral content similar to that in sound enamel and porosity which amounts to 1-2% [1,31].

Bioglass, as an external source of mineral ions, reacts rapidly when contacting with body fluid by releasing ions and raising the pH, forming crystals similar to natural HA [32]. In the present study, chitosan was introduced as the vehicle to carry the released ions from bioglass particles either as the pre-treatment or in the form of chitosan-bioglass complexes. The fact that chitosan can stabilise amorphous calcium phosphate (ACP) and induce transformation into HA, might potentiate its ability to benefit subsurface remineralisation [33]. Raman intensity mapping is a non-destructive method to quantify the mineral content change in the same sample area (**Figure S3**). The mineral content on lesion surfaces of CB and CBS in the static study showed a limited regain compared to RS as shown in **Table 2**. This is because of the co-precipitation of calcium phosphate and silicon phosphate. This is further evidenced by the high content of silicon on these surfaces (**Table 4**). When mechanical agitation was introduced, silicon was absent from the surface and the Ca/P ratios were close to that in pure HA, suggesting the precipitation was predominantly composed of apatitic phases. The greater mineral regains in both CB and CBS after pH-cycling also implied that chitosan contributed to remineralisation under clinically simulated conditions, perhaps by the mechanism previously reported [33]. Moreover, chitosan-bioglass complexing exhibited the most surface deposition. The pilot study suggested that the preparation of the chitosan-bioglass complex might lead to the formation of chitosan-ACP clusters confirmed by infrared spectroscopy and SEM (**Figure S1** and **Figure S2**). These ACP crystals were further transformed to HA, whereas in CB it is likely that some ACP crystals had crystallised to hydroxycarbonate apatite (HCA) [34] before being stabilised by chitosan, making it easy to be rinsed off and hence accounting for the reduction in surface mineral regain. Interestingly, silicon was also detected on the subsurface post-static remineralisation (**Table 4**) and the content in CBS was greater than that in CB, indicating that chitosan could carry ions into deeper lesions, concurring with Arnaud et al [24]. Remineralisation took place afterwards which is proved by the Ca/P ratio higher than that in RS and NC (**Table 3**).

The superiority of chitosan-bioglass complexing in remineralisation was further revealed by microhardness and SEM evaluations. In both remineralisation models, CBS exhibited significantly greater surface and subsurface hardness than deionised water treated lesions (**Figure 2** and **Figure 3**), indicating that CBS complex successfully strengthened the structure by occluding the porosities. Because chitosan is charged, there could be chemical bonding between newly precipitated minerals and the demineralised enamel. This is in agreement with Yamaguchi et al. who suggest that the chemical reaction between hydroxyapatite and chitosan is the consequence

of coordination bonds between metal ions (Ca^{2+}) and amino groups in chitosan [35]. In the present study, the "standard" remineralisation solution mimics saliva chemically with similar ions. RS didn't show significantly improved hardness than CB and CBS in all cases, which is in agreement with a previous report [36].

Tian et al. introduced chitosan gel to synthesize hydroxyapatite and proposed an organic model in which chitosan plays a crucial role, similar to type-I collagen in bone formation to orientate crystal growth [21]. Ruan et al. repaired demineralised enamel assisted with chitosan hydrogel and found a newly deposited mineral layer showing a porous morphology assembled by orientated crystals [26]. Current results, however, indicate that CB and CBS formed a dense surface structure composed of nano-sized crystals in both experiments (**Figure 4** and **Figure 5**), without any regulation of amelogenins. The spheres found in CBS after static remineralisation could be co-precipitated calcium phosphates and calcium silicate. This can be seen from the Ca/P ratio which is too high for calcium phosphate and the increased Si content. Despite the dense surface precipitation, subsurface mineralisation was observed. Crystals in CB are randomly distributed and reveal either spherical (static) or flaky (pH-cycling) morphologies. In CBS samples, the remineralised subsurface was denser than in that in CB. Surprisingly, after pH-cycling, it was found that precipitation covered the entire subsurface area, leaving no enamel prismatic structure exposed. This demonstrated that CBS is more effective in occluding subsurface porosities. Moreover, large plate-like crystals were also formed. The mechanism is unclear, but it may be postulated, as illustrated in **Figure 8**, that chitosan clusters carrying ACP are small enough to penetrate through the surface layer into the remaining voids and bond onto the walls of the demineralised prisms by a coordination bond reaction [35]. These clusters provide nucleation sites for apatitic crystals to grow and crystallise to form HA. This may also apply to explain the increased Ca/P ratios of CB and CBS post pH-cycling. These morphological findings are contrary to Ruan et al [26,27].

Despite the apparent efficacy of chitosan-bioglass to repair subsurface lesions, it should be noted that chitosan-bioglass complexes in the current study were prepared in the form of slurries, which might improve the kinetics compared to a hydrogel. In addition, the existence of pellicle didn't prevent chitosan-bioglass penetrating in both studies, suggesting a potential clinical application. Nevertheless, it is worth mentioning that pH-cycling study in the present work was only carried out for 7 days. Cochrane et al. recommends studies to be conducted for at least 6 months [14].

Furthermore, the artificial lesions created by the acidic gel models used, are considered to be more vigorously demineralised "high-R" lesions that are more responsive to differences in remineralising agents [37].

5. Conclusions

The null hypothesis was rejected. Chitosan-bioglass complex slurry was investigated as to its efficacy for repairing artificial enamel white spot lesions as compared to a chitosan pre-treatment method using static and dynamic (pH-cycling) remineralising protocols. Significant increase in surface mineral regain and hardness recovery were observed alongside dense precipitations on the lesion surfaces after treating with CBS in both studies. Specifically, subsurface porosities were filled with newly grown crystals after pH-cycling for 7 days. Ca/P ratio indicated the subsurface precipitation has a composition close to pure hydroxyapatite. It is proposed that the subsurface remineralisation by CBS is attributed to chitosan's ability to stabilise and carry amorphous calcium phosphate into deep lesion which can transform into HA phase with the remineralisation proceeds. The 3-minute in vitro pellicle layer did not significantly inhibit the remineralisation potential of CBS, but the mechanisms remained to be explored. Further investigations including interactions between the pellicles and remineralising agents as well as in vivo biofilm are a necessity.

Tables

Table 1 Composition of materials used in the study

Material	Compositions
BG slurry (1 g/L)	NovaMin^{TM} 4516 bioactive glass [a] (1 g), deionised water (1 mL)
Chitosan-BG slurry (0.5 g/ml)	NovaMin^{TM} 4516 bioactive glass [a] (1 g), chitosan solution (2 mL)
Chitosan solution (2.5 mg/mL)	Chitosan powder (25 mg), 0.1 M acetic acid solution (10 mL)
"Standard" remineralisation solution	HEPES (20 mM), KCl (130 mM), $CaCl_2$ (1.5 mM), KH_2PO_4 (0.9 mM), pH adjusted to 7.0 by 1 M NaOH
Artificial saliva	$CaCl_2$ (0.7 mM), $MgCl_2$ (0.2 mM), KH2PO4 (4.0 mM), HEPES (20 mM), KCl (30.0 mM), pH adjusted to 7.0 by 1M NaOH

[a] GlaxoSmithKline Healthcare (Weybridge, UK)

Table 2 Change of surface Raman intensity (ΔI, Mean (S.D.)) at 960 cm^{-1}. "*" indicates significant difference compared to NC in each study.

	CB	CBS	RS	NC
Static	5.11 (1.69)*	5.01 (1.64)*	9.07 (1.37)*	0.00 (0.72)
pH-cycling	10.20 (1.30)	14.46 (1.98)*	7.57 (1.78)	8.48 (2.22)

Table 3 Surface and subsurface Ca/P atomic ratios (Mean (S.D.)) of all groups post treatments. "*" indicates significant difference compared to NC ($p < 0.05$).

	Static		pH-cycling	
	Surface	Subsurface	Surface	Subsurface
CB	1.89 (0.03)	1.83 (0.18)	1.69 (0.03)	1.68 (0.15)
CBS	2.98 (0.38)*	1.67 (0.04)	1.68 (0.04)	1.68 (0.13)
RS	1.69 (0.01)	1.48 (0.04)	1.84 (0.19)	1.57 (0.03)
NC	1.70 (0.03)	1.57 (0.02)	1.75 (0.04)	1.59 (0.10)

Table 4 Surface and subsurface Ca/Si atomic ratios (Mean (S.D.)) of all groups post treatments. "*" indicates significant difference compared to CBS ($p < 0.05$).

	Static		pH-cycling	
	Surface	Subsurface	Surface	Subsurface
CB	16.31 (3.04)	14.86 (1.59)	-	-
CBS	5.04 (0.28)*	9.86 (0.93)*	-	-
RS	-	-	-	-
NC	-	-	-	-

Figures

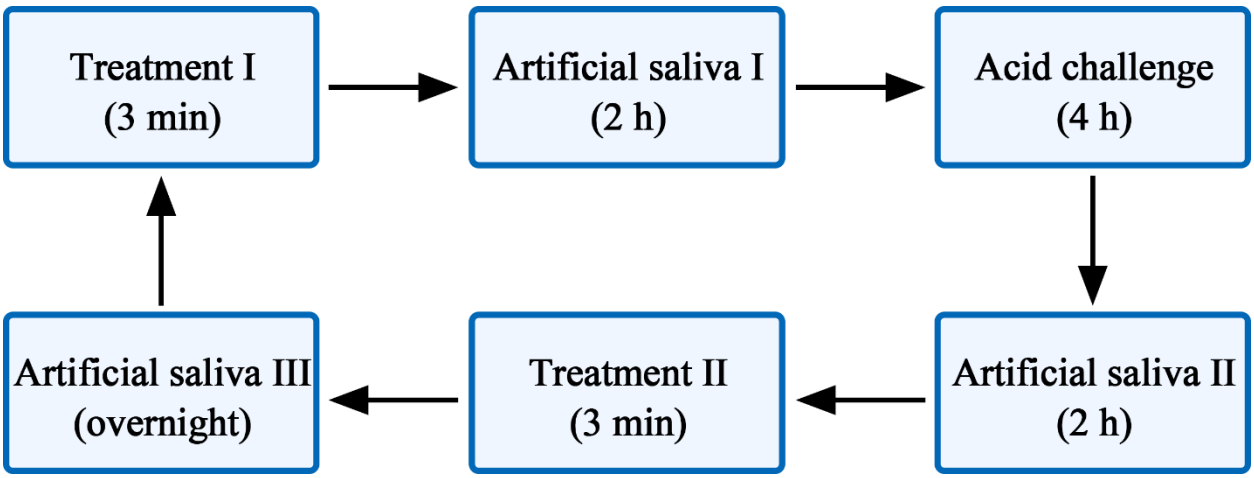

Figure 1 Illustration of pH-cycling. The entire regime lasted for 7 days.

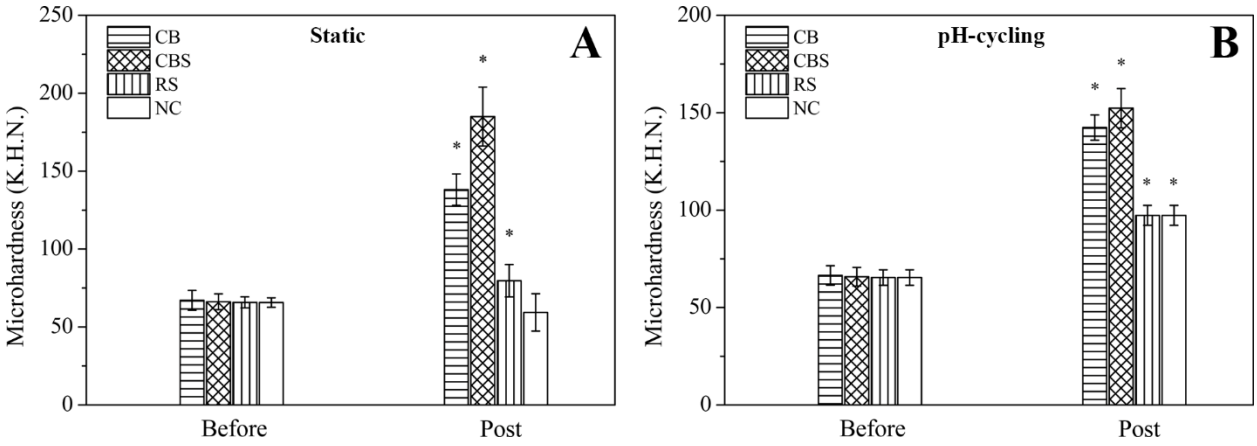

Figure 2 Surface Knoop microhardness of all groups before and post static (a) and pH-cycling (b) remineralisation regime (mean ± S.D., KHN). "*" indicates significant difference compared to the baseline value ($p < 0.05$). Before treatment, baseline microhardness reached around 65 which is accordance with previous reports. In static model (a), all groups except NC show obvious hardness recovery, in which CBS has the greatest performance (185.0 ± 18.9), whereas in NC the hardness decreased to 59.4 ± 12.0. In pH-cycling model (b), SMH significantly increased in all groups post treatment. In addition, CB (142.4 ± 6.5) and CBS (152.3 ± 10.1) reveal significantly greater hardness compared to NC (97.3 ± 5.1) ($p < 0.05$).

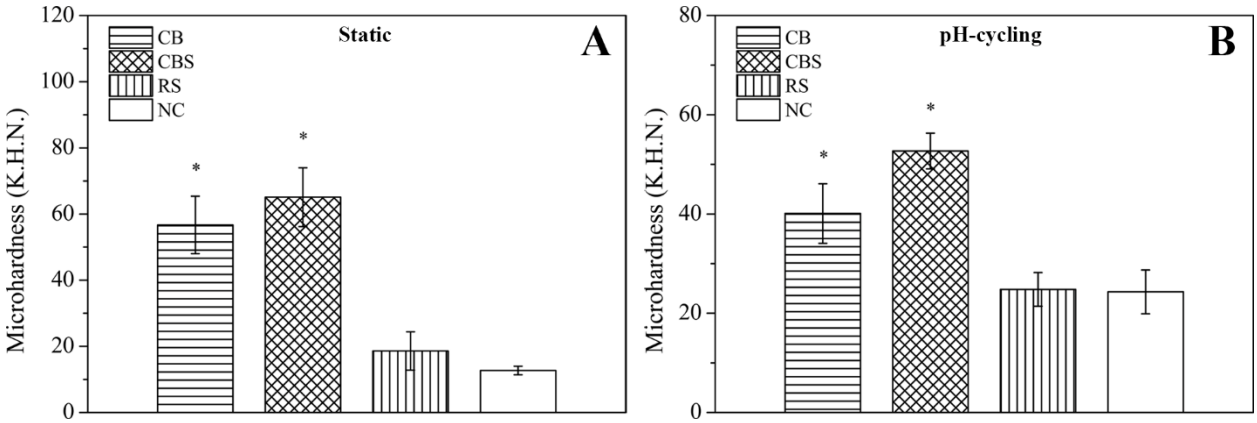

Figure 3 Subsurface (20 μm below) Knoop microhardness of all groups post static (a) and pH-cycling (b) remineralisation regime (mean ± S.D., KHN). "*" indicates significant difference compared to NC ($p < 0.05$). In both remineralisation models, CB and CBS exhibit significantly better mechanical performance compared to NC ($p < 0.05$). Additionally, the hardness values in CBS are slighter greater than those in CB, although this is not statistically significant ($p > 0.05$). RS group, in comparison, fails to exhibit obvious difference when compared to NC.

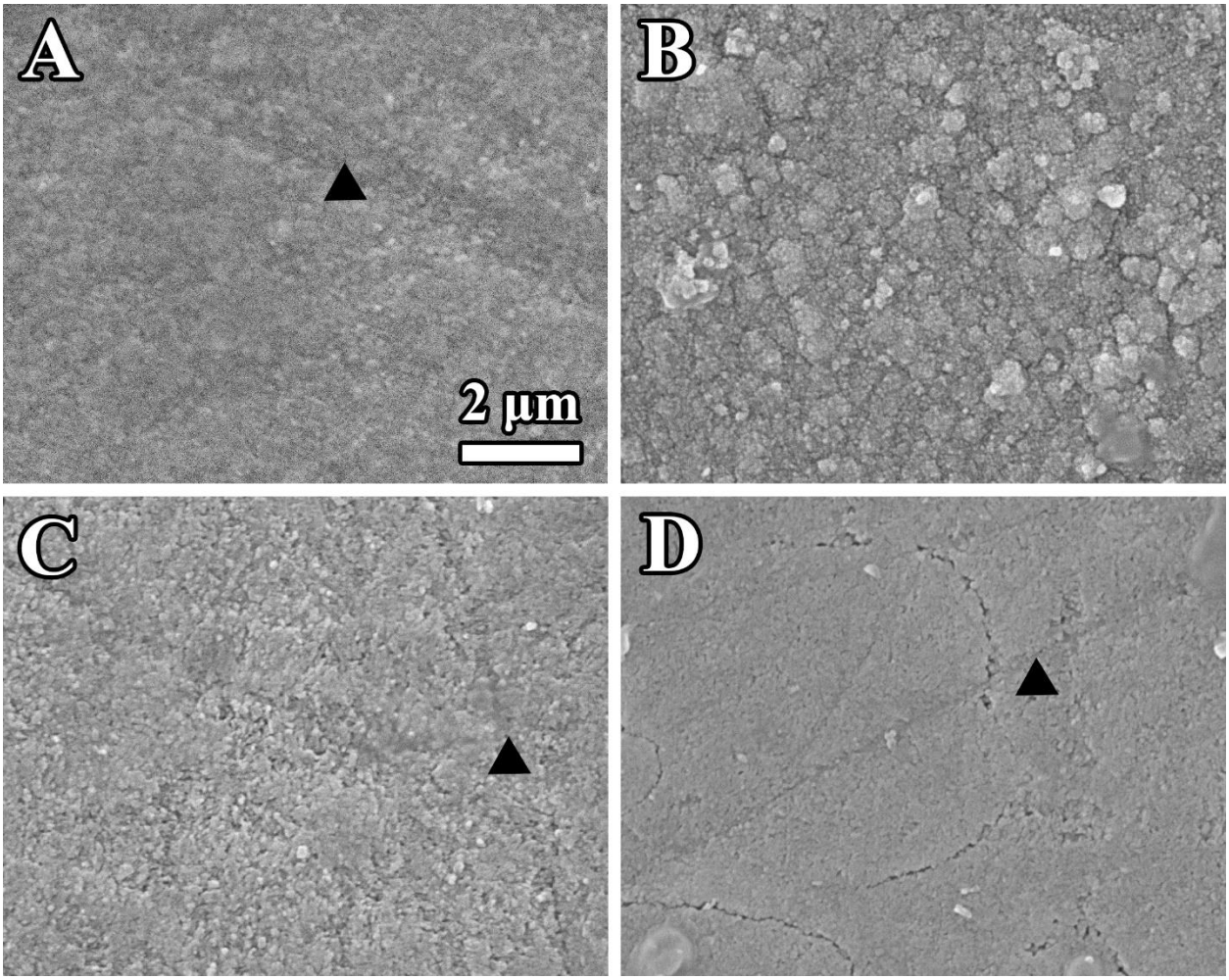

Figure 4 SEM observations (x10000) of the lesion surface after 7d static remineralisation. CS (a) exhibits a dense surface morphology with small crystals. RS (c) shows similar precipitation, however, the structure is more porous than that in CS as indicated by red arrows. Both surfaces preserved the scratching marks (black triangles). Interestingly, CBS (b) reveals significantly different features. A large number of micro-spheres composed of nanocrystals homogeneously covered the entire lesion surface. No scratch was observed. In comparison, samples treated by deionised water (d) shows no obvious precipitation of newly grown crystals except a few small depositions. In addition, the outline of enamel prism can be clearly seen in NC, which was absent in the other groups.

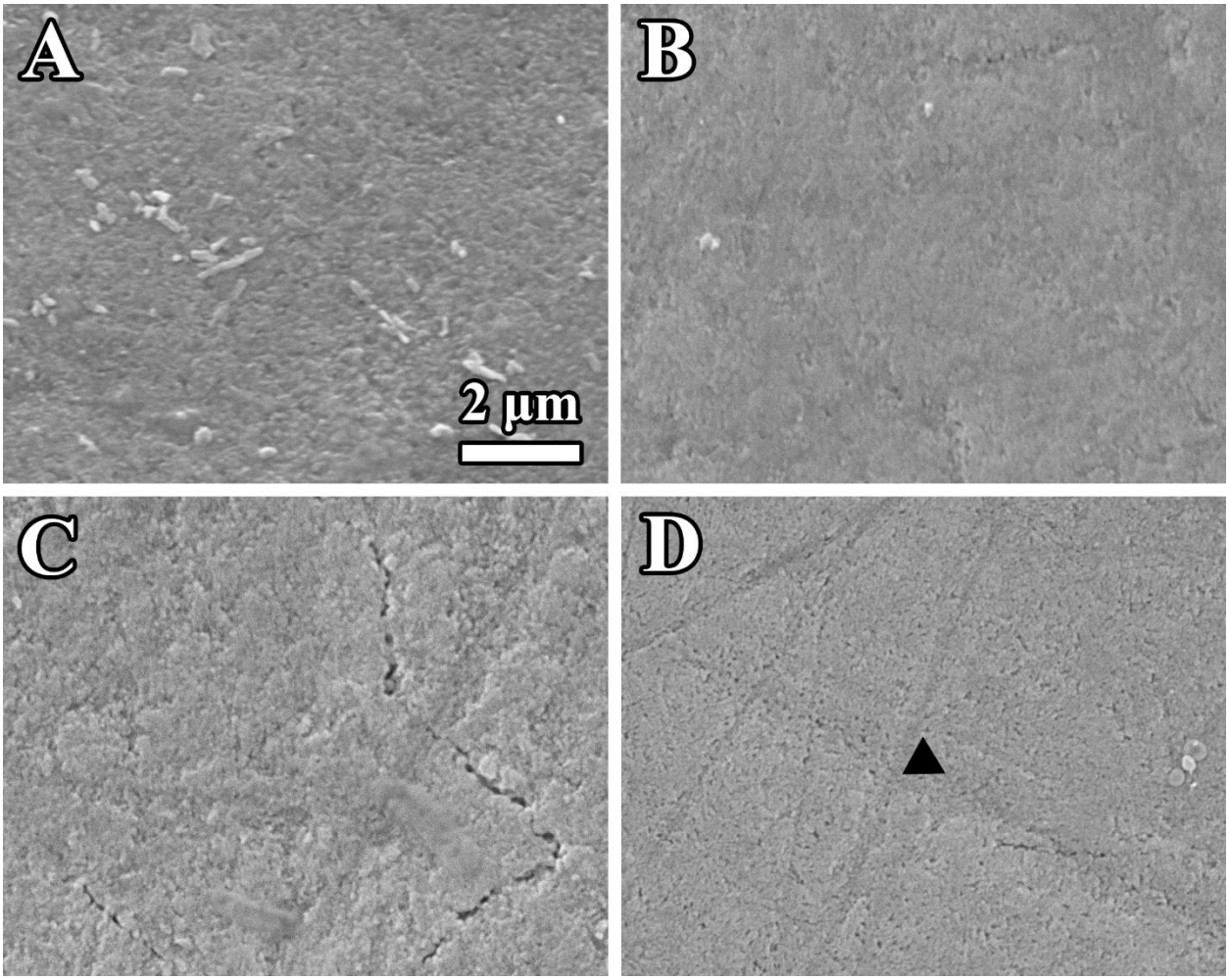

Figure 5 SEM observations (x10000) of the lesion surface after 7d pH-cycling. CS (a) shows a dense surface with some small depositions. Similarly, in CBS (b), the surface is covered by newly precipitated mineral layer. Compared to CS (a), this mineral layer in CBS (b) looks smoother and the crystal size is smaller. No obvious pores were observed in both groups. Precipitation was also found in RS (c) group. However, minerals were not homogeneously distributed. Prism outline was clearly seen, indicating the mineral layer is not as thick as that in CS and CBS. There was no clear sign of newly grown mineral and the surface remained porous in NC (d). In addition, scratches (black triangle) existed in both RS and NC groups after pH-cycling, whereas were absent in CB and CBS.

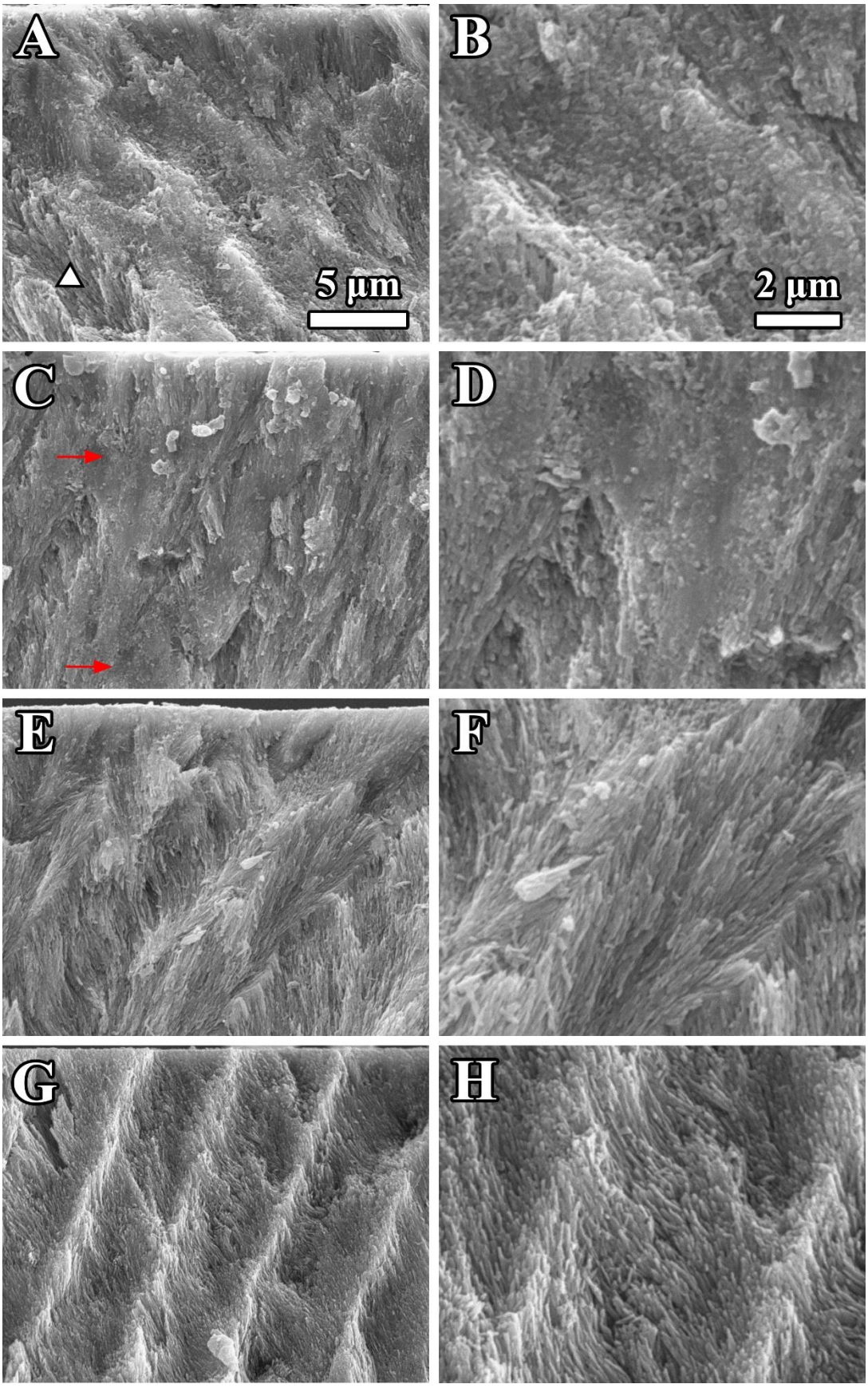
A
5 µm
B
2 µm
C
D
E
F
G
H

Figure 6 SEM observations (x4000 and x10000) of the lesion subsurface after 7d static remineralisation. Obvious mineral precipitation was observed in CB (a) and the coverage is across the entire subsurface investigated. Magnified observation (b) reveals that the precipitation layer was composed of round short crystals. Nevertheless, the precipitation is heterogeneous as porous prismatic structure was also found (white triangle). Similarly, patchy newly grown minerals were found in CBS (c) across the subsurface (red arrows). Enlarged micrograph (d) exhibits that the precipitation has a denser morphology compared to that in CB. Areas not covered by the precipitation shows a less porous structure than CB. In comparison, such kind of mineral layer was not seen in RS (e) and NC (g), in which classic prismatic structure was recognised with orientated crystals. Despite the absence of patchy precipitation, the structure was more porous in NC than that in RS. From the comparison between (f) and (h), it could be seen that crystals in RS were more tightly packed whereas in NC porosities were clearer.

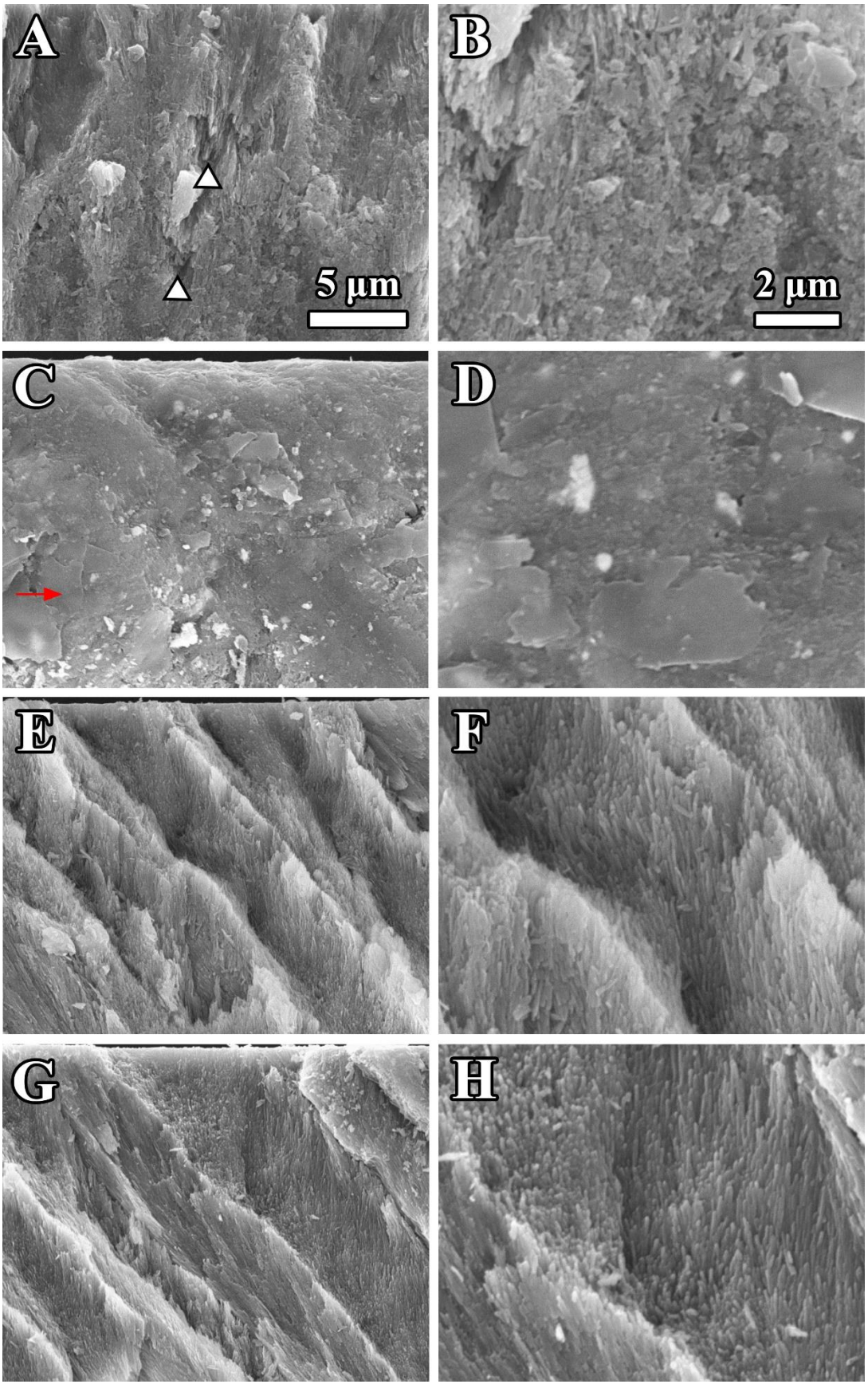
A
5 µm
B
2 µm
C
D
E
F
G
H

Figure 7 SEM observations (x4000 and x10000) of the lesion subsurface after 7d pH-cycling. In CB (a) and CBS (c) groups, classic prismatic structure was completely absent, which inversely could be clearly seen in RS (e) and NC (g). Precipitations were heterogeneously distributed on the subsurface of CB (a), leaving some pores open (white triangles). Crystals were flaky and loosely packed as can be seen from (b). In comparison, newly grown minerals covered the entire subsurface observed and no significant porosities were recognised in CBS group (c). Some large plate crystals up to 5 μm were also found (red arrow). The magnified investigation (d) reveals that newly grown nanocrystals were tightly packed, showing a dense morphology. No obvious sign of newly grown mineral was found in either RS (e) and NC (g). From (f) and (h), it can be seen that orientated crystals were loosely packed with some porosities.

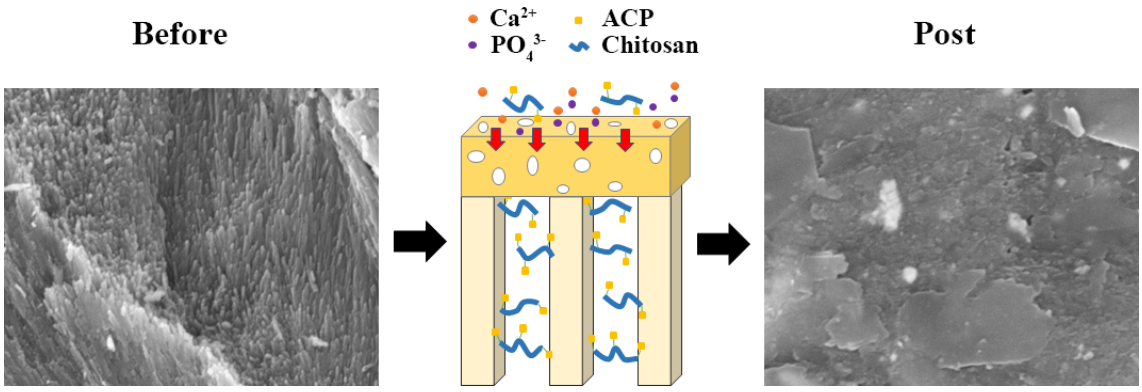

Figure 8 Schematic of mechanism of chitosan-bioglass complex in remineralising subsurface lesions.

Supporting Information

Infrared spectra of pure bioglass, chitosan powder, and chitosan-bioglass complexes with different concentrations; SEM micrographs of chitosan-bioglass complexes; and representative Raman intensity map of the same area before and after 7d pH-cycling in CBS group.

References

[1] C. Robinson, R.C. Shore, S.J. Brookes, S. Strafford, S.R. Wood, J. Kirkham, The chemistry of enamel caries, Crit. Rev. Oral Biol. Med. 11 (4) (2011) 481-495.

[2] E.A.M. Kidd, O. Fejerskov, What constitutes dental caries? Histopathology of carious enamel and dentin related to the action of cariogenic biofilms, J. Dent. Res. 83 (2004) C35-C38.

[3] R.H. Selwitz, A. Ismail, N.B. Pitts, Dental caries, Lancet. 369 (9555) (2007) 51-59.

[4] R.J.M. Lynch, S.R. Smith, Remineralization agents – new and effective or just marketing hype?, Adv. Dent. Res. 24 (2) (2012) 62-67.

[5] S. Twetman, S. Axelsson, H. Dahlgren, A.K. Holm, C. Källestål, F. Lagerlöf, P. Lingström, I. Mejàre, G. Nordenram, A. Norlund, L.G. Petersson, B. Söder, Caries-preventive effect of fluoride toothpaste: a systematic review, Acta Odontol. Scand. 61 (6) (2003) 347-355.

[6] D.T. Zero, Dentifrices, mouthwashes, and remineralization/caries arrestment strategies, BMC Oral Health. 6 (Suppl1) (2006) S9.

[7] S.B. Huang, S.S. Gao, H.Y. Yu, Effect of nano-hydroxyapatite concentration on remineralization of initial enamel lesion in vitro, Biomed. Mater. 4 (3) (2009) 034104.

[8] P. Tschoppe, D. Zandim, P. Martus, A.M. Kielbassa, Enamel and dentine remineralization by nano-hydroxyapatite toothpastes, J. Dent. 39 (6) (2011) 430-437.

[9] M. Hashimoto, M. Iijima, F. Nagano, H. Ohno, K. Endo, Effect of monomer composition on crystal growth by resin containing bioglass, J. Biomed. Mater. Res. B Appl. Biomater. 94 (1) (2010) 127-133.

[10] A.S. Bakry, H. Takahashi, M. Otsuki, J. Tagami, Evaluation of new treatment for incipient enamel demineralisation using 45S5 bioglass, Dent. Mater. 30 (3) (2014) 314-320.

[11] H. Milly, F. Festy, T.F. Watson, I. Thompson, A. Banerjee, Enamel white spot lesions can remineralise using bio-active glass and polyacrylic acid-modified bio-active glass powders, J. Dent. 42 (2) (2014) 158-166.

[12] J.M. ten Cate, J. Arends, Remineralization of artificial enamel lesions in vitro: III. A study of the deposition mechanism, Caries Res. 14 (6) (1980) 351-358.

[13] E.C. Reynolds, F. Cai, P. Shen, G.D. Walker, Retention in plaque and remineralization of enamel lesions by various forms of calcium in a mouthrinse or sugar-free chewing gum, J. Dent. Res. 82 (3) (2003) 206-211.

[14] N.J. Cochrane, D.T. Zero, E.C. Reynolds, Remineralization models, Adv. Dent. Res. 24 (2) (2012) 129-132.

[15] N.J. Cochrane, F. Cai, N.L. Huq,; Burrow, M.F.; Reynolds, E.C. New approaches to enhanced remineralization of tooth enamel, *J. Dent. Res*. 89 (11) (2010) 1187-1197.

[16] B.T. Amaechi, Remineralization therapies for initial caries lesions, Curr. Oral Health Rep. 2 (2) (2015) 95-101.

[17] M. Rinaudo, Chitin and chitosan: Properties and applications, Prog. Polym. Sci. 31 (7) (2006) 603-632.

[18] Y. Lin, R. Zheng, H. He, H. Du, Y. Lin, Application of biomimetic mineralization: A prophylatic therapy for crack teeth?, Med. Hypotheses. 73 (4) (2009) 493-494.

[19] M. Dash, F. Chiellini, R.M. Ottenbrite, E. Chiellini, Chitosan – a versatile semi-synthetic polymer in biomedical applications, Prog. Polym. Sci. 36 (8) (2011) 981-1014.

[20] H. Lee, S. Tsai, C. Kuo, A. W. Bassani, B. Pepe-Mooney, D. Miksa, J. Masters, J. Sullivan, R.J. Composto, Chitosan adsorption on hydroxyapatite and its role in preventing acid erosion, J. Colloid Interface Sci. 385 (1) (2012) 235-243.

[21] K. Tian, M. Peng, W. Fei, C. Liao, X. Ren, Induced synthesis of hydroxyapatite by chitosan for enamel remineralization, Adv. Mat. Res. 530 (2012) 40-45.

[22] P.M. Claesson, B.W. Ninham, pH-dependent interactions between adsorbed chitosan layers, Langmuir. 8 (5) (1992) 1406-1412.

[23] A. Young, G. Smistad, J. Karlsen, G. Rolla, M. Rykke, Zeta potentials of human enamel and hydroxyapatite as measured by the Coulter DELSA 440, Adv. Dent. Res. 11 (4) (1997) 560-565.

[24] T.M. Arnaud, B. de Barros Neto, F.B. Diniz, Chitosan on dental enamel de-remineralization: an in vitro evaluation, J. Dent. 38 (11) (2010) 848-852.

[25] J. Zhang, V. Boyes, F. Festy, R.J.M. Lynch, T.F. Watson, A. Banerjee, In-vitro subsurface remineralisation of artificial enamel white spot lesions pre-treated with chitosan, Dent. Mater. 34 (8) (2018) 1154-1167.

[26] Q. Ruan, Y. Zhang, X. Yang, S. Nutt, J. Moradian-Oldak, An amelogenin-chitosan matrix promotes assembly of an enamel-like layer with a dense interface, Acta Biomater. 9 (7) (2013) 7289-7297.

[27] Q. Ruan, J. Moradian-Oldak, Development of amelogenin-chitosan hydrogel for in vitro enamel regrowth with a dense interface, J. Vis. Exp. 89 (2014) 51606.

[28] Q. Ruan, D. Liberman, R. Bapat, K.B. Chandrababu, J.H. Phark, J. Moradian-Oldak, Efficacy of amelogenin-chitosan hydrogel in biomimetic repair of human enamel in pH-cycling systems, J. Biomed. Eng. Inform. 2 (1) (2016) 119-128.

[29] I. Rehman, L.L. Hench, W. Bonefield, R. Smith, Analysis of surface layers on bioactive glasses, Biomaterials. 15 (10) (1994) 865-870.

[30] J. Zhang, R.J.M. Lynch, T.F. Watson, A. Banerjee, Remineralisation of enamel white spot lesions pre-treated with chitosan in the presence of salivary pellicle, J. Dent. 72 (2018) 21-28.

[31] A.I. Darling, The selective attack of caries on the dental enamel, Ann. R. Coll. Surg. Engl. 29 (6) (1961) 354-369.

[32] J.S. Wefel, NovaMin®: Likely clinical success, Adv Dent Res. 21 (1) (2009) 40-43.

[33] X. Zhang, Y. Li, X. Sun, A. Kishen, X. Deng, X. Yang, H. Wang, C. Cong, Y. Wang, M. Wu, Biomimetic remineralization of demineralized enamel with nano-complexes of phosphorylated chitosan and amorphous calcium phosphate, J. Mater. Sci. Mater. Med. 25 (12) (2014) 2619-2628.

[34] L.L. Hench, Bioceramics, J. Am. Ceram. Soc. 81 (7) (1998) 1705-1728.

[35] I. Yamaguchi, K. Tokuchi, H. Fukuzaki, Y. Koyama, K. Takakuda, H. Monma, J. Tanaka, Preparation and microstructure analysis of chitosan/hydroxyapatite nanocomposites, J. Biomed. Mater. Res. 55 (1) (2001) 20-27.

[36] A. Lussi, N. Schlueter, E. Rakhmatullina, C. Ganss, Dental erosion - an overview with emphasis on chemical and histopathological aspects, Caries. Res. 45 (Suppl 1) (2011) 2-12.

[37] R.J.M. Lynch, U. Mony, J.M. ten Cate, Effect of lesion characteristics and mineralising solution type on enamel remineralisation in vitro, Caries Res. 41 (4) (2007) 257-262.